Diagnostic and Interventional Imaging (2019) **100**, 279—285

ORIGINAL ARTICLE /*Research and new developments*

Temporal evaluation of the microwave ablation zone and comparison of CT and gross sizes during the first month post-ablation in swine lung

H. Kodama[a], **E. Ueshima**[a], **K. Howk**[b], **S.W. Lee**[b], **J.P. Erinjeri**[a,c], **S.B. Solomon**[a,c], **G. Srimathveeravalli**[a,*]

[a] *Department of Radiology, Interventional Radiology Service, Memorial Sloan-Kettering Cancer Center, 1275 York avenue, 10065 New York, USA*
[b] *Medtronic Inc, Massachusetts, USA*
[c] *Department of Radiology, Weill Cornell Medical College, New York, USA*

KEYWORDS
Ablation zone;
Computed tomography (CT);
Lung;
Preclinical study;
Microwave ablation (MWA)

Abstract
Purpose: The purpose of this study was to investigate the development and evolution of the microwave ablation (MWA) lesion in the normal lung by using a swine model at various time points and to compare post-procedural computed tomography (CT) and gross pathologic findings during the first month post-ablation.
Materials and methods: Twenty-seven percutaneous MWA procedures were performed on swine lungs at 100 W for either 2 min (low dose, 18 ablations) or 10 min (high dose, 9 ablations). Animals were sacrificed at either 2 days ($n = 5$) or 28 days ($n = 5$) after ablation. All animals underwent CT imaging immediate post-treatment and prior to sacrifice, with additional imaging at 7 and 14 days for the 28-day cohort. After euthanasia, lungs and trachea were removed *en bloc* and underwent gross pathology analysis.
Results: In both dose treatment groups, CT measurements of the ablation zone were maximum at Day 7 (low dose: 7.50 ± 3.08 cm^3; high dose: 24.87 ± 11.34 cm^3) and significantly larger compared to the immediate post-ablation measurements (low dose: 2.54 ± 1.81 cm^3; $P = 0.00011$; high dose: 9.14 ± 3.42 cm^3; $P = 0.00374$). No significant differences in dimensions were observed between CT and gross pathologic images for both high and low dose ablations in both cohorts.
Conclusion: The treatment zone following MWA in the lung can vary in the sub-acute setting, achieving largest size at 7 days post-treatment. Furthermore, measurements from CT closely matched with gross pathologic ablation size.

* Corresponding author.
E-mail address: srimaths@mskcc.org (G. Srimathveeravalli).

https://doi.org/10.1016/j.diii.2018.10.008

Thermal ablation techniques such as radiofrequency (RFA) and microwave ablation (MWA) are minimally invasive approaches that may be used as alternatives for patients who are not eligible for surgical resection [1]. By comparison with RFA, MWA theoretically is more efficient in delivering faster and higher heating temperatures, rendering them less susceptible to the ''heat sink'' effect and creating larger ablation volumes [2—5]. The potential of MWA to ablate lung tumors have been demonstrated in several preclinical [6—9] and human studies [10—14]. Indeed, it is yet to be clinically demonstrated whether MWA is more effective than RFA for treatment of tumors in randomized controlled trials [15].

Imaging techniques such as computed tomography (CT) are often utilized to determine the ablation volume and assess if the residual tumor requires retreatment [16,17]. This evaluation is most often performed immediately to within 24 hours of the initial ablation, every 1—4 months thereafter, and if necessary at longer intervals [18]. However, very limited data is available assessing the sequential changes in ablation zones within the sub-acute settings (i.e., within 1 month). In fact, it has been shown that following RFA of lung tumors, the ablated lesion size can vary in size and shape within one-week post-treatment [19—21]. Furthermore, there are very few studies that directly correlate the lesions appeared in CT to those that are observed in gross findings [17,22].

The purpose of this study was to investigate the development and evolution of MWA lesion in the normal lung by using a swine model at various time points and to compare post-procedural CT and gross pathologic findings during the first month post-ablation.

Materials and methods

MWA procedures were performed in an *in vivo* porcine lung model using Emprint™ Ablation System (Medtronic). The MWA system was powered by a 2450 MHz generator, and delivers a maximum power of 100 W [23]. It was designed to produce predictable, spherical ablation zones, that are not impacted by the inherent characteristics of surrounding target tissues [24]. This investigation is an extension of a previously published study [9] and was approved by the Institutional Animal Care and Use Committee (IACUC) and animals were housed in an Association for Assessment and Accreditation of Laboratory Animal Care (AALAC) accredited facility.

In vivo porcine lung ablation model

Ten Yorkshire swine (3—4 months old; weight range 50—70 kg) underwent percutaneous CT-guided MWA in the unilateral lung as described previously [9]. The animals were anesthetized and maintained using continuous inhalation of isoflurane throughout the procedure. CT imaging (Lightspeed® RTLS, GE Healthcare) was used for insertion of 2 or 3 ablation antenna per animal. Each antenna was used to create a single ablation, and energy delivery for ablation was performed sequentially. A total of 27 percutaneous MWA procedures were performed at 100 W for either 2 min (low dose, 18 ablations) or 10 min (high dose, 9 ablations). Animals were assigned to either a 2- or 28-day follow-up cohort ($n = 5$ in each group).

CT imaging and follow-up procedures

Unenhanced CT scans were performed prior to the ablation procedure. Unenhanced and dual phase (30 s and 90 s) contrast-enhanced CT scans were performed immediately (within 10 min of ablation [Day 0]) and at follow-ups to assess ablation zone evolution. Animals assigned to the 2-day cohort group underwent CT imaging at Day 2 (approximately 48 hours post-ablation) and were euthanized at Day 2. Animals in the 28-day cohort group underwent CT imaging at Days 7, 14, and 28 and were euthanized at Day 28. Parameters for CT scan were: 120 kV tube voltage, tube current as determined by automatic exposure control, 0.8 sec CT gantry rotation time, 0.9375 pitch factor, 1.25 mm image slice thickness, and 500 mm data collection diameter. The ablation zone on CT was defined as a non-enhancing region on the mediastinal window settings (width: 400 HU, length: 500 HU) at Days 2, 7, 14 and 28. For Day 0, the ablation zone was defined as the region demonstrating ground-glass opacity enclosed within a hyperattenuating rim using lung window settings (width: 1600 HU, length: 500 HU) since the ablation zones were not clearly visible on CT images under mediastinal settings. On CT imaging, the region of ground-glass appearance was considered necrotic while the peripheral hyper-enhancing region was considered inflammatory rim. Two-dimensional measurements of ablation zones were performed on CT images in the transverse plane, in a slice corresponding to the microwave antenna insertion plane parallel to the insertion tracts.

Long- and short-axis diameters were recorded and the ablation volume at each time point was calculated assuming the ablation zone to be roughly ellipsoidal in shape:

$$Volume = \frac{\pi}{6}(SAD)^2(LAD)$$

where SAD and LAD represents short- and long-axis diameters, respectively. Data for Day 0 in both cohorts were pooled for analysis. These measurements were used to estimate the evolution of the post-treatment ablation zone.

Gross pathologic analysis

Animals were euthanized for gross analysis. Briefly, an intubation tube was placed into the trachea and the whole lungs were fixed by instillation of 10% neutral buffered formalin solution into the airway with pressure of 0.04 MPa for 30 min. Animal lungs and trachea were harvested *en bloc* and lung tissues containing the ablation were dissected free from surrounding tissues. The fixed tissues were processed by sectioning samples that were approximately 3—5 mm thick and cross-sections were photographed with an identification label and measurement reference. Each gross image was analyzed using the computer image analysis software. The gross samples from Days 2 or 28 time point were compared to CT imaging data from corresponding time point. Large slides were prepared to capture the entire ablation zone corresponding to the largest cross-section on imaging. H & E stained samples were evaluated by a board-certified

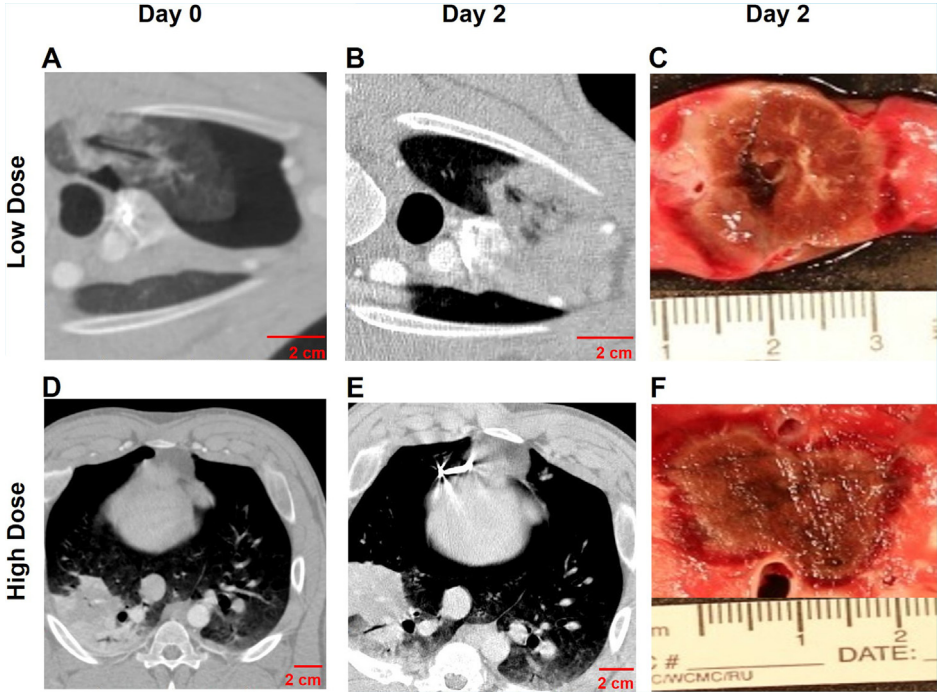

Figure 1. Measurements of the ablation zone. Sequential changes of the mean volume measurements of the ablation zone across following (A) low and (B) high dose MWA. Compared with CT taken immediately (within 10 minutes) after ablation, the size of the ablation zone peaks at Day 7. Comparison of mean CT and gross specimen volume ablation zone measurements for both (C) 2-day and (D) 28-day cohorts. No statistical significant difference was observed between CT and gross measurements. *denotes statistical significance ($P < 0.05$ vs. Day 0).

veterinary pathologist for measurements. However, some histological slides could not be measured because the size of the lesions impeded the whole section measurements.

Statistical analysis

Ablation zone size measurements were described using descriptive statistics. All measurements were expressed as means ± standard deviations (SD). Comparisons of ablation zone size at different time points were compared using unpaired Student *t* test, and the association between CT and gross findings were compared using a paired Student *t* test. All statistical analysis was conducted using EZR software (Saitama Medical Center, Jichi Medical University), which is a graphical user interface for R (The R Foundation for Statistical Computing, Vienna, Austria). *P*-values < 0.05 were inferred as evidence of statistical significance.

Results

Pneumothoraces occurred in 3 of 10 swine as reported in our previously published study [9]. Pneumothorax in 1 animal was stabilized using a flutter valve while the other 2 required continuous air drainage to maintain lung expansion. Hence, these 2 animals were sacrificed within 4 hrs after ablation, resulting in 8 swine that had evaluable data ($n = 4$ in both cohorts). In the 2-day cohort, there was evaluable data for a total of 4 high dose procedures (100 W, 10 min) and 6 with low dose (100 W, 2 min) ablation. In the 28-day cohort, data was available for 4 and 8 ablation procedures with high and low dose, respectively.

Dynamical evolution of the ablation zone

No significant changes in two-axis measurements (long- and short-axis diameters) and volume of the ablation zone were observed between Days 0 and 2 when the lung tissue was ablated at either low or high dose (Fig. 1). On Day 7, the measurements significantly peaked, and then subsequently decreased at later time points. Ablation volumes at Days 0 and 7 was 9.14 ± 3.42 (SD) cm^3 (range: 4.11—15.40 cm^3) vs. 24.87 ± 11.34 (SD) cm^3 (range: 14.09—40.87 cm^3) after high dose treatment ($P = 0.00374$) and 2.54 ± 1.81 (SD) cm^3 (range: 0.43—5.89 cm^3) vs. 7.50 ± 3.08 (SD) cm^3 (range: 3.23—12.63 cm^3) ($P = 0.00011$) after low dose treatment, respectively (Table 1).

CT imaging of ablation zone vs. gross pathologic specimen measurements

Figs. 2 and 3 show representative CT and gross images for both 2- and 28-day cohorts, respectively, at low and high dose (Table 2). For the 2-days cohort, the ablation volumes at low dose were 3.04 ± 1.72 (SD) cm^3 with CT (range: 1.04—5.59 cm^3) vs. 1.95 ± 1.32 (SD) cm^3 (range: 0.58—3.94 cm^3) with gross ($P = 0.234$); high dose were 11.30 ± 4.42 (SD) cm^3 (range: 6.07—16.86 cm^3) with CT vs. 7.64 ± 2.83 (SD) cm^3 (range: 3.84—10.63 cm^3) with gross ($P = 0.127$). In the 28-days cohort, the volumes for low dose were 0.78 ± 0.58 (SD) cm^3 (range: 0.20—1.49 cm^3) with CT vs. 0.67 ± 0.0.59 (SD) cm^3 (range: 0.09—1.61 cm^3) with gross ($P = 0.669$); high dose were 7.52 ± 8.15 (SD) cm^3 with CT (range: 1.71—19.32 cm^3) vs. 7.52 ± 9.02 (SD) cm^3 (range: 1.15—20.55 cm^3) with gross ($P = 0.999$).

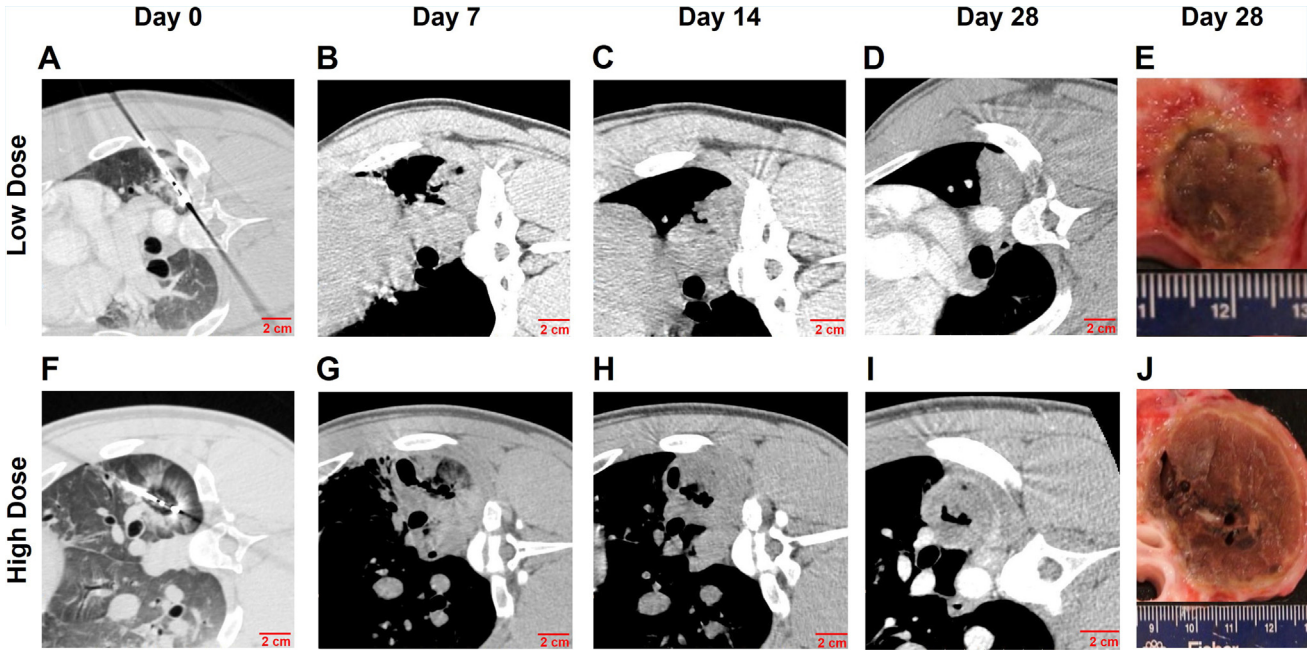

Figure 2. Representative CT and gross images of ablation zones following microwave ablation in the 2-day cohort. Serial changes of CT lung images at low (A—B) and high power (D—E). CT images of the ablation zone was taken at Day 0 (A, D) and within 2 days after ablation (B, E). After lung tissue fixation, gross images (C, F) were taken and ablation zone size were measured and compared with CT images at Day 2.

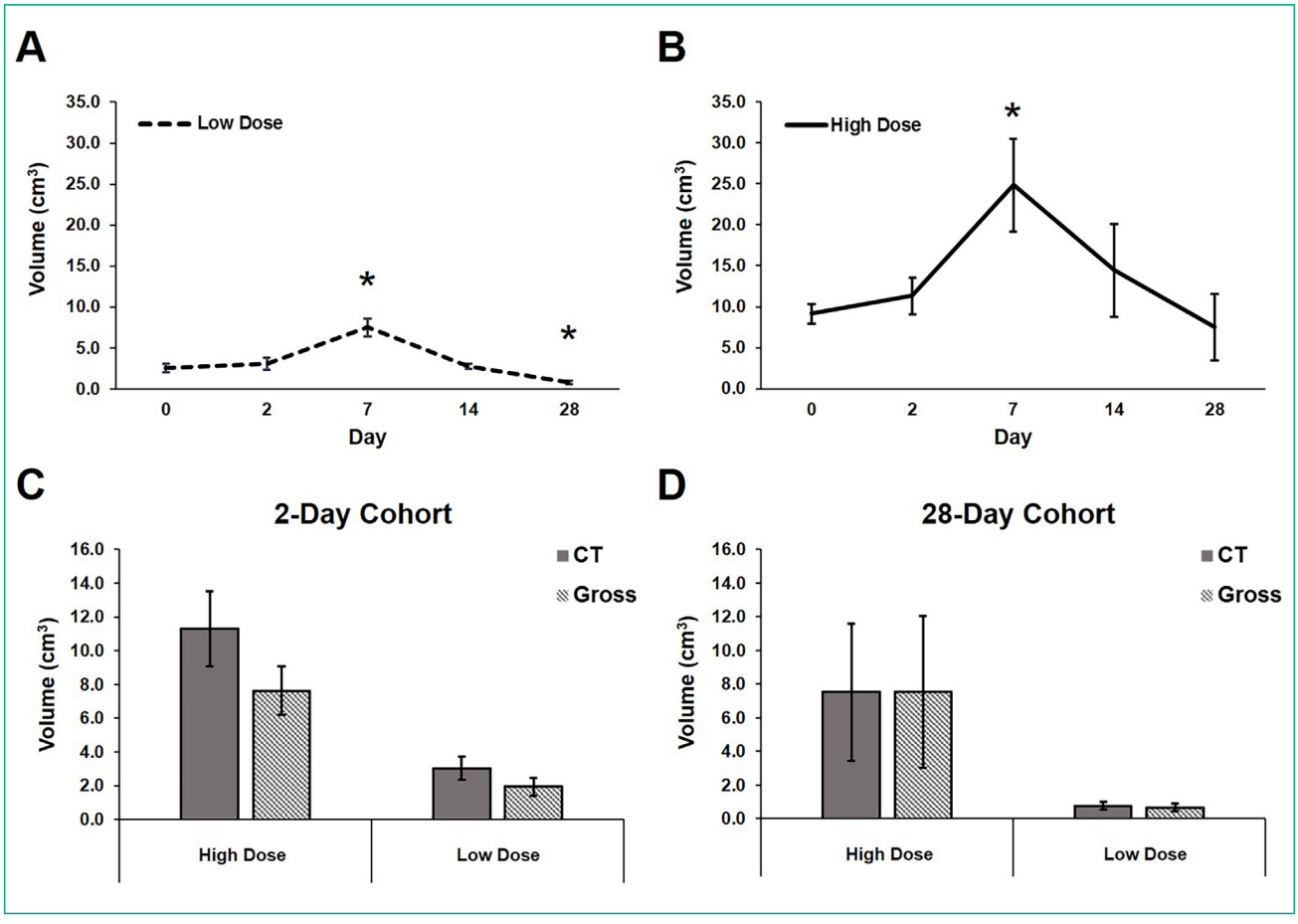

Figure 3. Representative CT and gross images of ablation zones following MWA in the 28-day cohort. Sequential monitoring of CT images of swine lungs at low (A—D) and high (F—I) dosage. CT images were taken at Day 0 (A, F), Day 7 (B, G), Day 14 (C, H), and Day 28 (D, I). Gross images of the lungs were taken at Day 28 (E, J) and compared with CT images at Day 28.

Table 1 Measurements of short-axis, long-axis, and volume of the ablation zone over time on computed tomography.

	Day	Short-axis diameter (cm)	Long-axis diameter (cm)	Volume (cm^3)
Low dose				
	0	1.35 ± 0.43 [0.71–1.97]	2.24 ± 0.45 [1.38–2.90]	2.54 ± 1.81 [0.43–5.89]
	2	1.52 ± 0.32 [1.07–1.96]	2.30 ± 0.48 [1.73–2.78]	3.04 ± 1.72 [1.04–5.59]
	7	2.10 ± 0.36 [1.49–2.60]	3.14 ± 0.74 [2.31–4.60]	7.50 ± 3.08 [3.23–12.63]
	14	1.53 ± 0.26 [1.19–1.98]	2.14 ± 0.18 [1.93–2.43]	2.71 ± 0.93 [1.48–4.06]
	28	0.96 ± 0.32[0.57–1.38]	1.34 ± 0.29 [0.94–1.76]	0.78 ± 0.58 [0.20–1.49]
High dose				
	0	2.26 ± 0.34 [1.73–2.92]	3.30 ± 0.46 [2.62–3.82]	9.14 ± 3.42 [4.11–15.40]
	2	2.44 ± 0.39 [1.95–2.82]	3.50 ± 0.55 [3.01–4.05]	11.30 ± 4.42 [6.07–16.86]
	7	3.12 ± 0.43 [2.73–3.72]	4.67 ± 0.85 [3.61–5.64]	24.87 ± 11.34 [14.09–40.87]
	14	2.68 ± 0.64 [2.03–3.55]	3.38 ± 0.94 [2.56–4.71]	14.45 ± 11.33 [6.28–31.08]
	28	2.04 ± 0.79 [1.29–3.12]	2.58 ± 0.94 [1.72–3.79]	7.52 ± 8.16 [1.71–19.32]

Data are presented as mean ± standard deviation. Numbers in brackets are ranges.

Table 2 Raw computed tomography and gross pathology volume measurements for both 2-day and 28-day cohorts.

	Ablation ID	CT volume (cm^3)	Gross volume (cm^3)	Histopathological volume (cm^3)
2-day cohort				
Low dose				
	2	1.037	1.809	4.608
	4	1.563	0.579	4.241
	12	4.005	3.944	7.756
	13	2.268	2.974	NA
	18	3.797	0.646	2.36
	19	5.592	1.726	4.347
High dose				
	1	6.073	3.836	5.542
	3	11.404	7.677	12.315
	11	10.869	10.631	11.454
	17	16.864	8.404	7.851
28-day cohort				
Low dose				
	6	0.366	0.265	NA
	7	0.261	1.115	0.761
	9	1.486	1.614	1.642
	10	1.466	0.357	0.413
	21	0.906	1.339	NA
	22	1.303	0.295	NA
	24	0.228	0.304	NA
	25	0.202	0.088	NA
High dose				
	5	19.317	20.548	10.799
	8	6.597	6.575	5.368
	20	2.452	1.149	NA
	23	1.708	1.805	NA

NA: not available due to size of the lesions impeding the whole section measurements.

Discussion

Given the theoretical advantages that MWA has over other thermal modalities, MWA has been widely used and reported to an efficient treatment for malignant primary and metastatic lung tumors with a low adverse event profile [2–14]. Despite its widespread clinical use, a number of knowledge gaps exist. This present study is the first to investigate the impact of MWA on healthy swine lung tissue and the temporal dynamics of its subsequent recovery through monitoring of the treatment zone during the first month post-ablation.

By comparison with surgical resection, the ablated tumor is not excised but rather left *in situ* following MWA therapy. Post-procedural CT is used to gauge the success of treatment and guide further management after thermal ablation [16,17,25,26]. Currently, there is a lack of information on the MWA zone during the first month post-ablation. Patients at most institutions either undergo post-ablation CT immediately or at 1 month after the procedure to determine if retreatment is necessary and/or to serve as a new baseline, followed by every one to three months thereafter and if necessary, at longer intervals [25,26]. Our present investigation aims to provide further insights into the evolution of the ablation zone during follow-up, specifically the first month.

Studies have previously reported conflicting results in terms of tissue characteristics following ablation procedures: some have reported tissue shrinkage during the ablation (e.g. 15—50%) [27,28] or the ablation zone may increase during the first 24 hours followed by subsequent reduction at later time points [25,26,28]. It is still an ongoing topic of research but tissue shrinkage is thought to occur due to dehydration, protein denaturation, and contraction of collagen [27,28] while rehydration of tissue, bleeding and subsequent inflammation are other contributing factors that may contribute to ablation zone changes during the acute phase [29—31]. Even though the present investigation is in general agreement with the finding that the lung tissue does indeed dynamically change over time, a significant peak in the post-ablation zone size at Day 7 has not been reported previously. Based on this observation, radiologists should not be alarmed that the size of the ablation appears to be large within one-week post-ablation and that the size will indeed change at subsequent time points. Hemorrhage, ensuing inflammation and cell apoptosis around the ablation zone from the heat energy applied may explain this observed phenomenon [29—31]. Nonetheless, additional experimental studies to precisely pinpoint the mechanistic process involved are warranted.

While no significant differences were observed in the treatment zone sizes following MWA when comparing CT and gross measurements, there was an approximately 50% difference between the two measurements, this could be due to our small animal sample size and the sectioned slice may not correspond to the largest cross-sectional imaging. Nonetheless, this finding suggests that CT, especially when obtained at 28 days after ablation, may accurately demarcate and map the boundary of the ablation zone.

The limitations of our study include the small sample size and that ablations were performed in healthy swine lungs rather than tumors, and thus, it is uncertain if these results may be directly translated to humans with lung tumors. Gross pathology assessment was also relatively insufficient as intermediary time points (7, 14, and 21 days) were not collected. Additionally, we did not perform a multivariable analysis to account for animals contributing for more than one ablation.

In conclusion, in addition to that the volume of MWA ablation may vary over the course of the one- month follow-up period, our study provides the first evidence that the size of the MWA lesion in the lung significantly peaks at 7 days post-ablation irrespective of the duration of energy delivered in a porcine model. Our results also demonstrated no significant differences between CT and gross pathology measurements of the ablation zone. Future studies are warranted to investigate the mechanisms involved during the dynamic evolution of the ablation zone in order to provide further insights into the therapeutic efficacy of MWA and aid in the development of a reliable, standardized post-procedural assessment of the *in vivo* ablation size.

Ethics approval

All applicable international, national, and/or institutional guidelines for the care and use of animals were followed. All procedures performed in studies involving animals were in accordance with the ethical standards of the institution or practice at which the studies were conducted.

Funding

This study was funded by Medtronic, Inc. and the NIH Cancer Center Support Grant (P30 CA008748) for core laboratory services used for the experimental studies.

Acknowledgement

The authors would like to acknowledge Mamata Thapa, PhD (Medtronic, Inc.) for providing medical writing support and Sebastien Monette, DMV, MVSc (Memorial Sloan-Kettering Cancer Center) for histopathological measurements.

Disclosure of interest

G. Srimathveeravalli received grant support from Medtronic, Inc. to perform the reported work.

S. B. Solomon is a consultant with Johnson & Johnson, BTG, AngioDynamics, GE Healthcare and Medtronic, Inc.

K. Howk and S. W. Lee are employees of Medtronic, Inc. The other authors have no conflict of interests to report regarding the work reported in this manuscript.

The other authors declare that they have no competing interest.

References

[1] de Baere T, Tselikas L, Catena V, Buy X, Deschamps F, Palussiere J. Percutaneous thermal ablation of primary lung cancer. Diagn Interv Imaging 2016;97:1019—24.

[2] Brace CL. Microwave tissue ablation: biophysics, technology and applications. Crit Rev Biomed Eng 2010;38:65—78.

[3] Hines-Peralta AU, Pirani N, Clegg P, Cronin N, Ryan TP, Liu Z, et al. Microwave ablation: results with a 2.45-GHz applicator in ex vivo bovine and in vivo porcine liver. Radiology 2006;239:94—102.

[4] Simo KA, Tsirline VB, Sindram D, McMillan MT, Thompson KJ, Swan RZ, et al. Microwave ablation using 915-MHz and 2.45-GHz systems: what are the differences? HPB (Oxford) 2013;15:991—6.

[5] Lubner MG, Brace CL, Hinshaw JL, Lee FT. Microwave tumor ablation: mechanism of action, clinical results and devices. J Vasc Interv Radiol 2010;21:S192—203.

[6] Planche O, Teriitehau C, Boudabous S, Robinson JM, Rao P, Deschamps F, et al. In vivo evaluation of lung microwave ablation in a porcine tumor mimic model. Cardiovasc Intervent Radiol 2013;36:221—8.
[7] Brace CL, Hinshaw JL, Laeseke PF, Sampson LA, Lee Jr FT. Pulmonary thermal ablation: comparison of radiofrequency and microwave devices by using gross pathologic and CT findings in a swine model. Radiology 2009;251:705—11.
[8] Crocetti L, Bozzi E, Faviana P, Cioni D, Della Pina C, Sbrana A, et al. Thermal ablation of lung tissue: in vivo experimental comparison of microwave and radiofrequency. Cardiovasc Intervent Radiol 2010;33:818—27.
[9] Kodama H, Ueshima E, Gao S, Monette S, Paluch LR, Howk K, et al. High power microwave ablation of normal swine lung: impact of duration of energy delivery on adverse event and heat sink effects. Int J Hyperthermia 2018;34:1186—93.
[10] Egashira Y, Singh S, Bandula S, Illing R. Percutaneous high-energy microwave ablation for the treatment of pulmonary tumors: a retrospective single-center experience. J Vasc Interv Radiol 2016;27:474—9.
[11] Splatt AM, Steinke K. Major complications of high-energy microwave ablation for percutaneous CT-guided treatment of lung malignancies: single-centre experience after 4 years. J Med Imaging Radiat Oncol 2015;59:609—16.
[12] Ierardi AM, Coppola A, Lucchina N, Carrafiello G. Treatment of lung tumours with high-energy microwave ablation: a single-centre experience. Med Oncol 2017;34:5.
[13] Liu H, Steinke K. High-powered percutaneous microwave ablation of stage I medically inoperable non-small cell lung cancer: a preliminary study. J Med Imaging Radiat Oncol 2013;57:466—74.
[14] Little MW, Chung D, Boardman P, Gleeson FV, Anderson EM. Microwave ablation of pulmonary malignancies using a novel high-energy antenna system. Cardiovasc Intervent Radiol 2013;36:460—5.
[15] Vietti Violi N, Duran R, Guiu B, Cercueil JP, Aube C, Digklia A, et al. Efficacy of microwave ablation versus radiofrequency ablation for the treatment of hepatocellular carcinoma in patients with chronic liver disease: a randomised controlled phase 2 trial. Lancet Gastroenterol Hepatol 2018;3:317—25.
[16] Chheang S, Abtin F, Guteirrez A, Genshaft S, Suh R. Imaging features following thermal ablation of lung malignancies. Semin Intervent Radiol 2013;30:157—68.
[17] Kim C. Understanding the nuances of microwave ablation for more accurate post-treatment assessment. Future Oncol 2018;14:1755—64.
[18] Vogl TJ, Nour-Eldin NA, Hammerstingl RM, Panahi B, Naguib NNN. Microwave ablation (MWA): basics, technique and results in primary and metastatic liver neoplasms — review article. Rofo 2017;189:1055—66.
[19] Yamamoto A, Nakamura K, Matsuoka T, Toyoshima M, Okuma T, Oyama Y, et al. Radiofrequency ablation in a porcine lung model: correlation between CT and histopathologic findings. AJR Am J Roentgenol 2005;185:1299—306.
[20] Goldberg SN, Gazelle GS, Compton CC, McLoud TC. Radiofrequency tissue ablation in the rabbit lung: efficacy and complications. Acad Radiol 1995;2:776—84.
[21] Ahrar K, Price RE, Wallace MJ, Madoff DC, Gupta S, Morello Jr FA, et al. Percutaneous radiofrequency ablation of lung tumors in a large animal model. J Vasc Interv Radiol 2003;14:1037—43.
[22] Awad MM, Devgan L, Kamel IR, Torbensen M, Choti MA. Microwave ablation in a hepatic porcine model: correlation of CT and histopathologic findings. HPB (Oxford) 2007;9:357—62.
[23] Ierardi AM, Mangano A, Floridi C, Dionigi G, Biondi A, Duka E, et al. A new system of microwave ablation at 2450 MHz: preliminary experience. Updates Surg 2015;67:39—45.
[24] Alonzo M, Bos A, Bennett S, Ferral H. The emprint™ ablation system with thermosphere™ technology: one of the newer next-generation microwave ablation technologies. Semin Intervent Radiol 2015;32:335—8.
[25] Kawamoto S, Permpongkosol S, Bluemke DA, Fishman EK, Solomon SB. Sequential changes after radiofrequency ablation and cryoablation of renal neoplasms: role of CT and MR imaging. Radiographics 2007;27:343—55.
[26] Palussiere J, Marcet B, Descat E, Deschamps F, Rao P, Ravaud A, et al. Lung tumors treated with percutaneous radiofrequency ablation: computed tomography imaging follow-up. Cardiovasc Intervent Radiol 2011;34:989—97.
[27] Park CS, Hall SK, Liu C, Payne SJ. A model of tissue contraction during thermal ablation. Physiol Meas 2016;37:1474—84.
[28] Brace CL, Diaz TA, Hinshaw JL, Lee FT. Tissue contraction caused by radiofrequency and microwave ablation: a laboratory study in liver and lung. J Vasc Interv Radiol 2010;21:1280—6.
[29] Smith SL, Jennings PE. Lung radiofrequency and microwave ablation: a review of indications, techniques and post-procedural imaging appearances. Br J Radiol 2015;88:20140598.
[30] Erinjeri JP, Thomas CT, Samoilia A, Fleisher M, Gonen M, Sofocleous CT, et al. Image-guided thermal ablation of tumors increases the plasma level of interleukin-6 and interleukin-10. J Vasc Interv Radiol 2013;24:1105—12.
[31] Ohno T, Kawano K, Sasaki A, Aramaki M, Yoshida T, Kitano S. Expansion of an ablated site and induction of apoptosis after microwave coagulation therapy in rat liver. J Hepatobiliary Pancreat Surg 2001;8:360—6.